Molecular BioSystems

This article was published as part of the

2008 Emerging Investigators Issue

Highlighting the work of outstanding young scientists at the chemical- and systems-biology interfaces

Please take a look at the full table of contents to access the other papers in this issue.

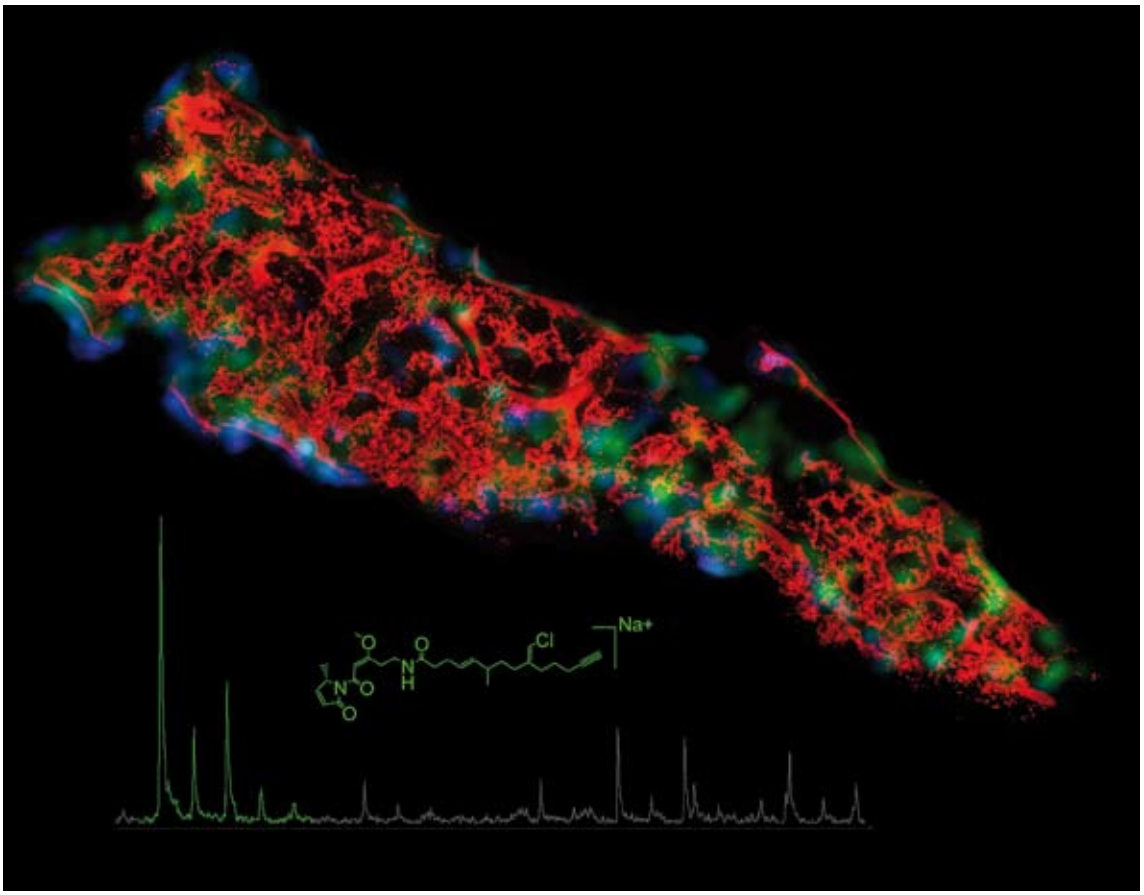

Accurate measurements of protein interactions in cells *via* improved spatial image cross-correlation spectroscopy†

Jonathan W. D. Comeau,[a] David L. Kolin[a] and Paul W. Wiseman*[ab]

Received 3rd January 2008, Accepted 26th March 2008
First published as an Advance Article on the web 16th April 2008
DOI: 10.1039/b719826d

The sensitive detection of protein interactions in living cells is an important first step toward understanding each of the multitude of cellular processes that are regulated by such interactions. Spatial image cross-correlation spectroscopy (ICCS) is one method used to measure protein–protein interactions from the analysis of two-channel fluorescence microscopy images. In spatial ICCS, cross-correlation of fluctuations in fluorescence intensity recorded as images from two independent wavelength detection channels in a fluorescence microscope is used to determine the average number of interacting particles in the imaged region. Even in situations where the particle number density is relatively high, ICCS provides an accurate measure of molecular interactions. However, it was shown previously that the method suffers from relatively high detection limits of interacting particles ($\sim$20%) and can be perturbed by heterogeneous spatial distributions of the fluorescent particles within the images. Here, we demonstrate new approaches to circumvent some of the limitations of ICCS. Spatial scrambling of pixel blocks within fluorescence images was investigated as a way of extending the detection of spatial ICCS to measure lower interaction fractions as well as colocalization within cells. We also show that 'mean-intensity-padding' of regions of interest within fluorescence images is a feasible method of applying ICCS to arbitrarily selected areas of the cell with boundaries or edge morphologies that would be impossible to analyze with conventional ICCS. Using these newly developed strategies we were able to measure the fraction of actin that interacts with α-actinin in the leading edge of a migrating cell.

1. Introduction

The measurement of the entire set of protein–protein interactions that drive most cellular functions is a daunting task that has only started to be achieved in last fifteen years with the development of high-throughput techniques such as two-hybrid screening.[1,2] These methods have provided the necessary tools to measure the complete interaction map of signaling networks, such as the integrin receptor 'adhesome' (Fig. 1),[3] as well as the entire interactome of the budding yeast, *Saccharomyces cerevisiae*.[4,5] Understanding the effect that the interconnected relationships between these proteins have on the overall functions of the cell itself is quickly emerging as a new paradigm in cell and systems biology. Although high-throughput screening approaches offer a wealth of information, the degree of specificity and sensitivity of these methods is a common concern,[6,7] as is the loss of spatial and temporal information with respect to the individual protein interactions *in situ*. These limitations necessitate the continued development and application of new techniques that are capable of fully characterizing the interaction between single protein complexes, especially with respect to membrane-associated protein interactions, which cannot be reliably measured using most high-throughput methods (see ref. 8 for a review).

A molecular binding event (covalent, electrostatic, *etc.*) inside a cell results in a number of measurable effects, which can be used to monitor the presence of such interactions. Changes in binding affinities,[9] secondary structural changes,[10] or reduced diffusion coefficients[11] are just some of the effects that have been observed following such binding events. Perhaps this is the reason why so many different techniques can be tailored to fit the particular detection needs of a given system. For example, surface plasmon resonance,[12] isothermal titration calorimetry,[13] mass spectrometry,[14] Raman spectroscopy,[15,16] and atomic force microscopy[17] have all been successful in measuring, and in some cases quantifying, the interaction between two proteins. None of these methods, however, has found as widespread application as fluorescence spectroscopy and microscopy, which are readily applicable to live cell measurements unlike some of the techniques mentioned above.

Most approaches for measuring the interaction of cellular constituents based on fluorescence microscopy require the labeling of two species with different fluorophores and imaging the emissions in two detection channels, which is then followed by an appropriate method of analyzing the collected images.

[a] *Department of Chemistry, McGill University, 801 Sherbrooke St., W. Montréal, Québec, Canada H3A 2K6. E-mail: jonathan.comeau@mcgill.ca. E-mail: david.kolin@mcgill.ca*
[b] *Department of Physics, McGill University, 3600 University St., Montréal, Québec, Canada H3A 2T8. E-mail: paul.wiseman@mcgill.ca*

† This article is part of a *Molecular BioSystems* 'Emerging Investigators' issue highlighting the work of outstanding young scientists at the chemical- and systems-biology interfaces.

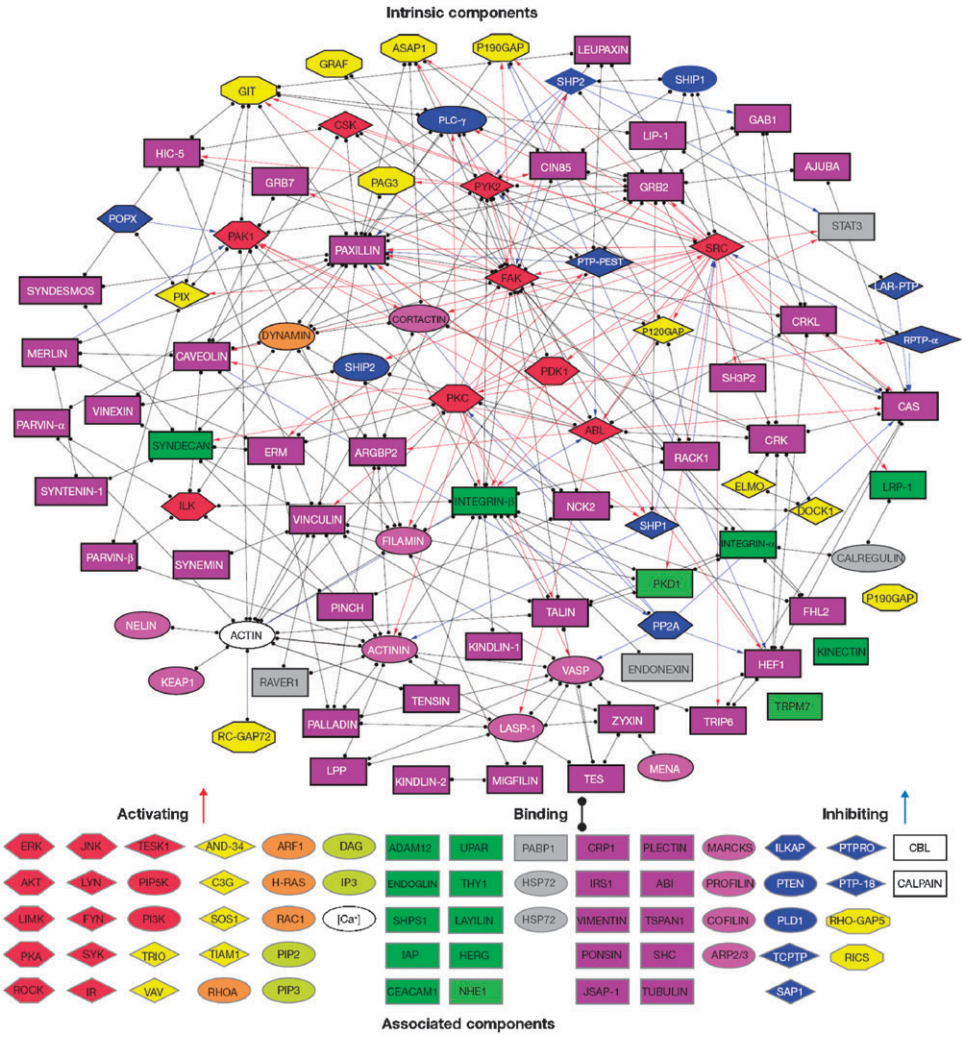

Fig. 1 Integrin membrane receptor proteins mediate cellular adhesion and signal transduction in many different cell types by direct and indirect association and recruitment of a vast array of proteins. Recently, the complete interaction network of integrin receptors was derived from previously published data and is an excellent illustration of the complexity involved in a just a small subset of the complete interactome of eukaryotic cells. Each line represents one of the 690 interactions between the 156 components. Reprinted by permission from Macmillan Publishers Ltd, *Nat. Cell Biol.* **9**(8) 858–867, copyright 2007.

One such method uses two fluorophores (donor and acceptor) with the appropriate spectroscopic properties such that Förster resonance energy transfer (FRET) will occur between the two labelled interacting species. FRET is often used as a direct measure of molecular interactions due to the extremely high sensitivity of the FRET efficiency on the separation distance (<10 nm) between the donor and acceptor-labelled macromolecules.[18] However, interpretation of FRET data in the presence of multiple donors and acceptors is often quite difficult and the reason why most FRET experiments are performed at low density labeling or on single donor–acceptor pairs. Another common image analysis technique involves statistical analysis of the two detection channel images for the presence of spatially overlapping signals, *i.e.* colocalization within pixels. This is typically accomplished by determination of an intensity threshold value which is subsequently used to classify all the pixels above this threshold as colocalized. The measurement of a high degree of colocalization indicates close proximity of the two labelled species, and therefore suggests a nonrandom interaction between the two labelled molecules of interest. This approach, pioneered by Manders' and co-workers, and similar variants, have been applied to numerous biological systems to establish the presence of colocalization, and therefore interaction, within fluorescence microscopy images.[19] Finally, we have shown that spatial correlation analysis of intensity fluctuations in fluorescence images collected *via* laser scanning microscopy (LSM) provides an accurate measure of the number (and fraction) of interacting particles within two-channel fluorescence microscopy images.[20] This technique, called image cross-correlation spectroscopy (ICCS), is particularly well suited for detecting and quantifying molecular interactions when the total particle number density of the system of interest is large.[21] In fact, the accuracy of ICCS was shown to be much greater than the common statistical colocalization analyses based on Manders'[19] or Pearson's correlation coefficients.[22]

Image cross-correlation spectroscopy was developed as a spatial variant of fluorescence cross-correlation spectroscopy

(FCCS),[23–25] which can measure the dynamic properties of interacting fluorescently tagged macromolecules in solution,[26,27] or in live cells.[28,29] Fluorescence intensity fluctuations that are recorded simultaneously in two spectrally-separated detection channels, and arise from changes in the fluorophore concentrations within a small observation volume defined by the beam focus of an excitation laser(s), are cross-correlated in time to reveal transport properties and number densities of any interacting and non-interacting species. In contrast, ICCS utilizes cross-correlation analysis of spatial (and temporal) intensity fluctuations in images collected *via* various fluorescence microscopy techniques, which allows for the measurement of the number densities and transport dynamics of molecules moving at much slower timescales (*e.g.* $D = 0$–$0.1\ \mu m^2\ s^{-1}$) than those accessible through FCCS. The slower timescales accessible by ICCS analysis are appropriate for measurements on fluorescently labelled membrane proteins,[30] or for quantifying the number of interacting immobilized proteins within fixed cells.[31] By demonstrating the ability of ICCS to accurately measure interacting particle number densities in single images at relatively high surface densities of the fluorophore, we have shown that the technique is a viable and important new tool for detecting protein colocalization in cells. For a fluorescence cross-correlation measurement, interacting species are those that are correlated in time or space within the diffraction-limited beam focal volume. Hence, molecular binding partners that are in direct contact and those that are not in direct contact, but are part of a common multimolecular complex, are by definition interacting. In most cases it is only the fraction of interacting species that is measured using these techniques, although equilibrium binding constants between directly associated proteins have been measured using both FCCS and ICCS.[21,32]

Although ICCS outperforms other statistical fluorescence colocalization methods, especially when the two labelled protein expression levels are different, the technique suffers from relatively high detection limits (*i.e.* the minimum fraction of interacting particles that can be measured).[21] As we will show, these detection limits depend strongly on the size of the area of analysis. In addition, large perturbations of the spatial correlation functions that are used to determine the number of interacting particles are introduced by nonuniform particle distributions, which can be the case in nuclear regions of the cell, or when observing elements of the cytoskeleton, or for confined morphologies such as filopodial extensions. In this work, we present new strategies for overcoming aspects of these limitations that significantly increase the range of applicability of ICCS for measuring intermolecular interactions within two-channel fluorescence microscopy images. Utilizing computer simulated two-color images, we were able to control the particle densities and interaction fractions, thus enabling a complete characterization of the ICCS interaction fraction detection limits. We show that spatially rearranging, or scrambling, the image prior to ICCS analysis significantly improves the dynamic range of the technique by increasing the reliability of the nonlinear fitting of the spatial correlation functions that is required in ICCS. By imaging a focal adhesion associated protein important in integrin activation, YFP-labelled talin, we demonstrate the implication of nonuniform particle distributions on spatial ICCS measurements and propose alternative solutions to the problem. Finally, we use these new strategies to measure the interaction fraction between actin–mRFP and α-actinin–GFP at the leading edge of a migrating cell using spatial ICCS.

2. Theory

In principle, ICCS can be applied to molecules that are free to move in three dimensions, but is typically performed on systems that are restricted to two dimensions (2D), such as proteins that are embedded in the planar cell membrane. The image collection is typically achieved by employing a confocal or two-photon laser scanning microscope (LSM), but practically any fluorescence imaging system would suffice. For two-channel confocal LSM imaging, two separate laser lines are rapidly scanned across the sample to excite two spectrally distinct fluorophores and the fluorescence emission is detected separately and recorded in 2D image pixel arrays. The scanning can also be repeated in time to generate an image time series.[30] With ICCS, therefore, two distinct types of fluorescence intensity fluctuations are recorded: spatial fluctuations as a function of pixel position within a given image (*i.e.*, a single time sample), and fluctuations in time defined for each pixel position through the entire image time series. This study deals with the analysis of single, two-channel images, and we will therefore only consider the spatial intensity fluctuations, $\delta i_k(x, y)$, within a given image in the discussion that follows. The spatial fluctuations recorded in channel k, $\delta i_k(x, y)$, are defined as the difference between the fluorescence intensity recorded at pixel position, (x, y), and the mean intensity of the image, $\langle i_k \rangle$:

$$\delta i_k(x,y) = i_k(x,y) - \langle i_k \rangle. \quad (1)$$

It should be noted that in this definition all the pixels in a given image are assumed to be recorded simultaneously, even though a typical 256×256 pixels image may take ~ 0.5 s to be acquired on a laser scanning microscope. This assumption is not problematic as long as the dynamics of the system of interest are slower than the image acquisition rate while correlations for those species that move faster than the imaging rate will be lost. It should be noted, however, that ICCS analysis of temporal image series will lead to determination of the transport properties and average number density of interacting fluorescently labelled molecules within the system. A thorough description of the theory detailing several image correlation methods that include temporal fluctuation analysis can be found in the original papers[30,33] and in a comprehensive review of image correlation techniques.[34]

The reciprocal of the number of particles per beam area (BA, defined by the spot area of the diffraction limited excitation laser focus) in channel k, including both interacting and noninteracting species, $\langle N \rangle_k$, is equal to the square relative fluctuation provided the fluctuations in fluorescence intensity are due only to particle concentration fluctuations and that the system is linear (*e.g.*, two fluorophores are twice as bright as one):

$$\langle N\rangle_k^{-1} = \frac{\langle(\delta i_k)^2\rangle}{\langle i_k\rangle^2}. \quad (2)$$

In practice, however, white noise sources contributing to every pixel intensity within the image prevent a direct calculation of the square relative fluctuation, thus necessitating its indirect evaluation *via* extrapolation of the best fit function to the zero-lags amplitude of the normalized spatial intensity fluctuation correlation function:

$$r(\xi,\eta)_{kl} = \frac{\langle \delta i_k(x,y)\delta i_l(x+\xi,y+\eta)\rangle}{\langle i_k\rangle\langle i_l\rangle}, \quad (3)$$

where ξ and η are spatial lag variables, and the subscripts k and l represent two distinct image detection channels. Eqn (3) is an autocorrelation function when $k = l$ and a cross-correlation function when $k \neq l$. In order to estimate the amplitude of the correlation functions, $r(0,0)_{kl}$, the auto- or cross-correlation functions are fit to a 2D Gaussian without weighting the zero spatial-lags point:

$$r(\xi,\eta)_{kl} = r(0,0)_{kl}\exp\left[-\frac{(\xi-\upsilon)^2+(\eta-\nu)^2}{\omega_0^2}\right] + r_\infty, \quad (4)$$

where the fit parameters are shown in bold and are the zero-lags amplitude, $r(0,0)_{kl}$, the e^{-2} laser beam radius, ω_0, the position of the peak maximum, (υ,ν), and an offset parameter, r_∞, to account for long-range spatial correlations. The number of interacting particles, $\langle N\rangle_{kl}$, can then be determined from the ratio of the cross-correlation amplitude to that of the autocorrelation amplitudes, provided there is no fluorescence quenching or enhancement upon binding of the fluorophores:

$$\langle N\rangle_{kl} = \frac{r(0,0)_{kl}}{r(0,0)_{kk}r(0,0)_{ll}}\frac{A_l}{A_k}. \quad (5)$$

The ratio of the effective areas defined by the focal spots of the two lasers ($A_l > A_k = \pi\omega_k^2$) is included in eqn (5) when the two excitation and detection volumes differ by a small amount,[35] and can be measured directly from the fitted beam radii for each detection channel. Finally, using eqn (5), we can define the ICCS interaction fractions (IFs), M_{ICCS}, as the ratio of the number of interacting particles to that of the total number of fluorescently labelled particles in each detection channel,

$$\begin{aligned} M1_{\mathrm{ICCS}} &= \frac{r(0,0)_{kl}}{r(0,0)_{ll}} = \frac{\langle N\rangle_{kl}}{\langle N\rangle_{kk}} \\ M2_{\mathrm{ICCS}} &= \frac{r(0,0)_{kl}}{r(0,0)_{kk}} = \frac{\langle N\rangle_{kl}}{\langle N\rangle_{ll}}. \end{aligned} \quad (6)$$

We refer to $M1_{\mathrm{ICCS}}$ and $M2_{\mathrm{ICCS}}$ as the ICCS colocalization coefficients because, similar to Manders' colocalization coefficients,[19] they provide a measure of the observed colocalization within the image regions analyzed. They also have the added advantage of direct determination of the absolute number densities of all interacting and non-interacting species.

3. Results and discussion

3.1 Improving the detection limits in ICCS

Due to the statistical nature of ICCS it is imperative that a sufficient number of independent spatial samples, *i.e.* fluctuations, be recorded to obtain meaningful results. As a measure of the number of samples present in a given image, we introduce a parameter called the number of independent fluctuations (NIF). The NIF is defined as the ratio of the total image area to the area of the beam focal spot (or Gaussian convolution function in computer simulated images), since the latter represents one fluctuation area sampled. It was determined previously that at NIF values of $\sim$1000, which corresponds to 256 × 256 pixel images at typical pixel resolutions of 0.1 μm per pixel ($\omega \approx 0.4$ μm), the zero spatial-lags amplitude of the cross-correlation function becomes indistinguishable from the background correlation peaks at all higher spatial lag values when the interaction fraction is <15%. Thus, when $\sim$1000 independent fluctuations are sampled within both of the images, the ICCS IF detection limit was determined to be 15%. Moreover, this detection limit was found to be independent of the total particle density.[21] In most experimental situations 15% would be an acceptable interaction fraction detection limit. The difference between 0, 2% or 5% interaction, for instance, is typically not significant in the context of biological systems due to the large cell-to-cell variability often encountered when measuring any parameter in cells. Of greater concern is the relatively large amount of sampling that is required to obtain such IF detection limits. Low sampling is a common obstacle encountered for ICCS measurements on various types of cells. For example, elongated fibroblast cells can easily spread out over areas >1000 μm^2, which corresponds to $\sim$2000 independent fluctuations. A problem arises, however, because in most cases, ICCS analysis over the entire cell is not an option, either because the particle distribution is nonuniform throughout the entire cell (to be discussed in detail later), or it is of interest to measure the amount of interaction in a particular subregion within the cell. In addition, other cell-types, such as cytotoxic T-cells for instance, are nearly 10 times smaller (<100 μm^2) than fibroblasts, which will significantly reduce the spatial fluctuation sampling across the cell (NIF $\sim$200).

In order to investigate the effect of spatial sampling on the minimum IF that can be detected using ICCS, sets of 20 image pairs were simulated with successively decreasing interaction fractions, but with the total particle densities in channels 1 and 2 held constant and equal at 8 particles/BA. The minimum interaction fraction was determined when more than half of the 20 trials returned failed fits of the two-dimensional Gaussian fit of the cross-correlation function. A failed fit was defined as a fitted e^{-2} beam radius outside a range of ±50% of the simulation input value, or when the fitted peak position, (υ,ν), was shifted by more than 2 pixels from the center, (ξ,η). This second criterion was included because it was found that in some instances, large off-center peaks would appear as well-defined Gaussian functions that would perturb the fitting of the central peak. This procedure was repeated for varying sample sizes (*i.e.* image areas) in order to determine the dependence of the IF detection limit on the NIF sampled.

As the size of the image (NIF value) decreases, the ICCS detection limit increases significantly (Fig. 2). The analysis of small image areas (NIF <50) is not possible unless the IF is very high (>40% in the case of a 64 × 64 pixel region). The analysis of such regions, which is often desired for the reasons

mentioned above, could easily give false-negative results when the true IF is quite large. One way to circumvent this problem is to increase the NIF by acquiring multiple images as a function of time and then performing spatial ICCS on each of the resulting two-channel image pairs. The total NIF sampled in the time series will increase provided the fluorescently labelled particles move (*e.g.*, diffusion or flow) between each successive image acquisition such that different spatial distributions of the particles can be sampled. For example, averaging three of the resulting spatial cross-correlation functions calculated between images that were acquired at three different points in time is equivalent to performing the cross-correlation analysis on a single image pair that is three times as large in area as the original images. Since the NIF is increased 3-fold in this case, the zero spatial-lags peak of the cross-correlation function will be better resolved. This averaging significantly facilitates the fitting procedure, thereby lowering the IF detection limit (Fig. 3).

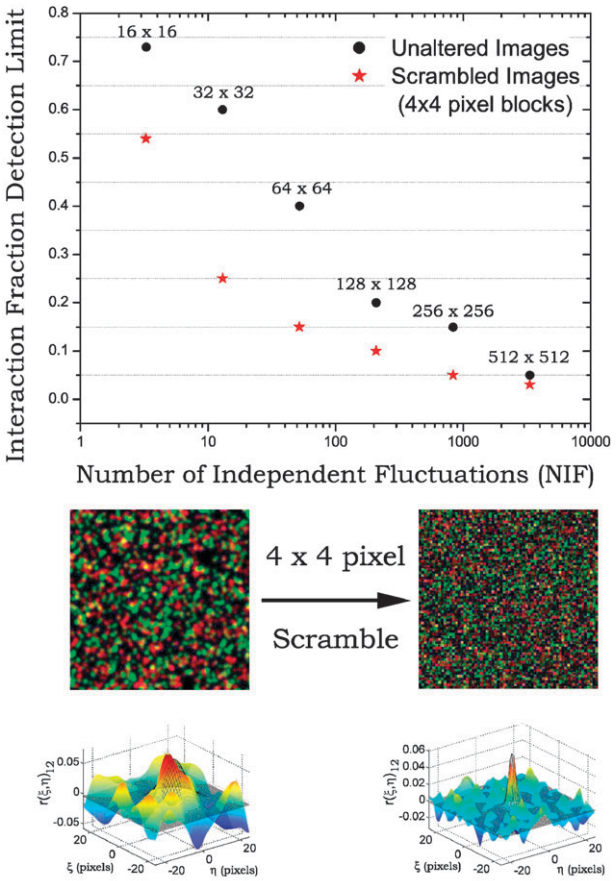

Fig. 2 The minimum interaction fraction that could be detected using ICCS analysis as a function of the number of independent fluctuations (NIF) in the simulated images for both unaltered and the corresponding scrambled image. Both channel particle densities were held constant and equal (8 particles/BA) as the number of interacting particles was decreased. The detection limit was defined as the IF at which more than half of the 20 trials returned a fitted e^{-2} beam radius outside a range of ±50% of the simulation input value, or a fitted peak position, (υ,ν), that was shifted more than 2 pixels from the center, (x,y). Shown below is an overlay image of a 256 × 256 pixel image (NIF ~ 800) with 10% interaction (below the detection limit) and the corresponding spatial cross-correlation function. The 4 × 4 pixel block scrambled image is also shown with the corresponding spatial cross-correlation function to demonstrate the much better 2D Gaussian fit when the image is randomly scrambled prior to ICCS analysis.

If however, acquiring multiple images in time is simply not an option due to the nature of the sample (*e.g.* fixed cell, slow moving particles, rapid photobleaching, *etc.*), then we propose an alternate approach to actually reduce the IF detection limits for a given NIF sampled. This will be described in the following section. As alluded to above, ICCS analysis fails to detect interaction fractions below the detection limits plotted in Fig. 2 because of the difficulty in fitting the cross-correlation function for such limited sampling. The zero spatial-lags amplitude of the cross-correlation function is not well resolved from the background correlation peaks at nonzero spatial lags, which significantly perturbs the fitting routine. An important observation, however, is that the value of the zero spatial-lags amplitude is still representative of the number of interacting particles even at several IFs values below the reported detection limits, it is just extremely difficult to extract this value from the 2D Gaussian fit. Thus it is worthwhile to investigate alternative methods for obtaining the cross-correlation zero spatial-lags amplitude.

Recall that the reason for fitting of the spatial autocorrelation function is the presence of the correlated white noise peak that is present at spatial lags of zero. In principle, however, the zero spatial-lags amplitude of the cross-correlation function could be calculated directly from the spatial intensity fluctuation data as there should be no cross-correlated white noise (by definition of this noise) present between the two detection channels:

$$r(0,0)_{kl} = \frac{\langle \delta i_k(x,y)\delta i_l(x,y)\rangle}{\langle i_k\rangle\langle i_l\rangle}. \qquad (7)$$

There are some other factors, however, that must be considered before deciding to abandon the spatial cross-correlation function fitting routine altogether. First, it is not uncommon that the peak of the spatial cross-correlation function occurs at spatial lags greater than zero, and the Gaussian fitting function allows for shifts in the cross-correlation peak. These pixel shifts can be due to small misalignments between the two detection channels.[36] These pixel shifts would introduce error into the direct calculation of the zero spatial-lags cross-correlation amplitude from the image pixels. Since this is the case, we could also determine the cross-correlation amplitude by searching for a local maximum at small spatial lag values to account for these small pixel shifts, although, due to the fact that multiple peaks are commonly observed at small spatial lags in low IF situations due to sampling noise, this method would be difficult. Secondly, the zero spatial-lags amplitude of the spatial cross-correlation function fails to be a good estimator of the average number of interacting particles at low enough IFs for a given NIF sampled. There will simply not be enough cross-correlated fluctuations to precisely measure these interactions. Therefore, fitting has the added advantage of providing a built-in check of the quality of the measurement, which the simple calculation directly from the pixel data of the zero-lags cross-correlation does not provide.

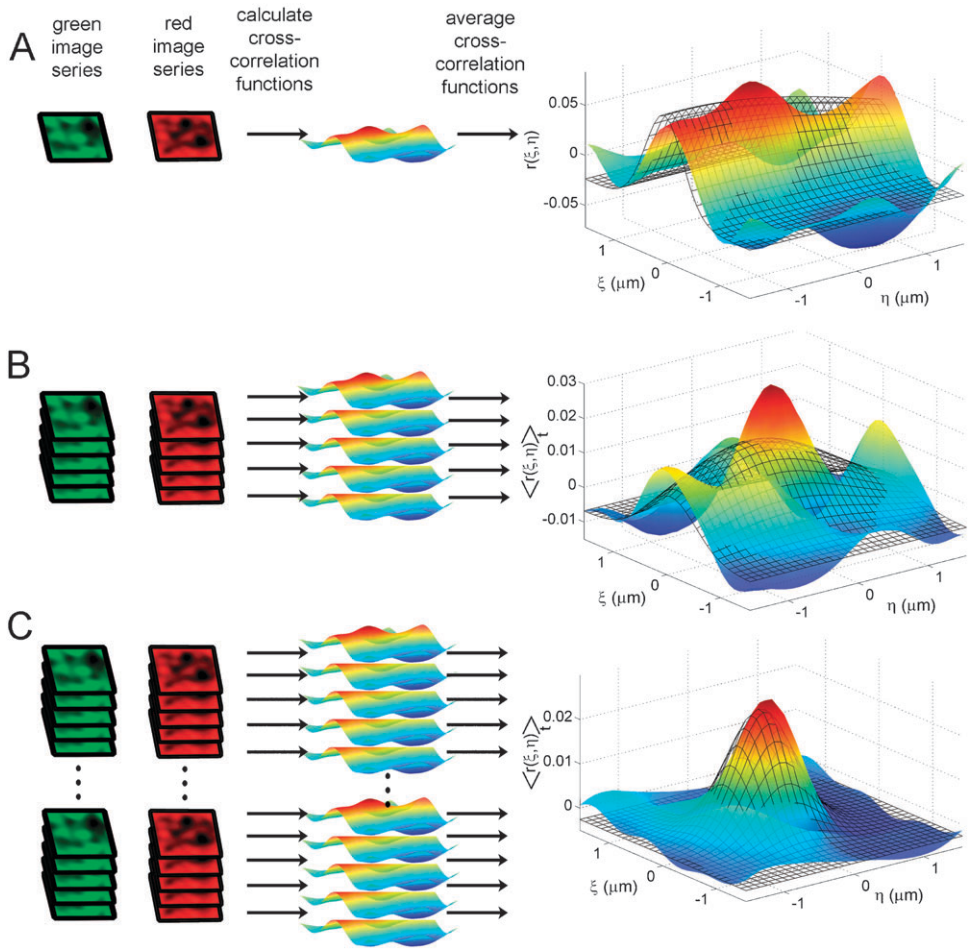

Fig. 3 A two-channel image time series of diffusing particles was simulated with total number densities of 8 particles/BA and an IF of 20%. (A) ICCS analysis of the first pair of images in the time series results in a poor fit of the spatial cross-correlation function due to a lack of spatial sampling (NIF = 13). By averaging the spatial cross-correlation functions calculated between the first 10 pairs of images (B) (NIF = 130), or the entire 100 pairs of images (C) (NIF = 1300), the central peak of the cross-correlation function is increasingly well-resolved due to the greater number of spatial samples.

3.2 Image scrambling for spatial ICCS

All information regarding the locations of the particles within an image is lost when a spatial correlation function is calculated from that particular image due to the averaging performed over all spatial lags. This implies that spatial rearrangement of all the pixels, or blocks of pixels, within an image, and subsequent spatial correlation, will result in an identical zero spatial-lags value as that of the unaltered image (see eqn (7)). Fig. 4 shows a schematic diagram of the image scrambling procedure. The only difference between the spatial auto- and cross-correlation functions calculated for a particular image and a spatially scrambled variant of that image, is the width of the correlation function decay, which in turn depends on the size of the scrambled motif. For example, scrambling all of the individual pixels in an image by randomly assigning each one of them a new location will destroy the inherent spatial correlation that was present prior to the rearrangement procedure (*i.e.* the particles were correlated with themselves over several pixels due to the fact that the diffraction-limited diameter of the focussed laser beam used to excite them was larger than the pixel size). In this case, the spatial correlation (at nonzero spatial lags) of the particles within the image was destroyed by the pixel scrambling. The spatial autocorrelation will have one peak at zero spatial lags (identical to the maximum of the peak that would result from correlation of the unscrambled image), and will effectively be a delta function. We can, however, preserve some of the spatial correlation of the particles within the image if instead of scrambling individual pixels, we divide the image into 2 × 2 pixel blocks, and then perform the random assignment of these blocks to new locations within the image. This time, the spatial autocorrelation function will only decay to zero after two spatial lags because the 2 × 2 pixel blocks are still spatially correlated after a shift of only one pixel (Fig. 5). The same will be true of the spatial cross-correlation function calculated between two images that were randomly scrambled in an identical fashion. Again, the zero spatial-lags value of the autocorrelation function for the scrambled image is identical to that of the unscrambled image, although the value at a spatial lag of one is lower for the autocorrelation of the scrambled image. By dividing the image into 2 × 2 pixel sections, and changing the position of these blocks, we have effectively thrown away several of the spatial lag = 1 values

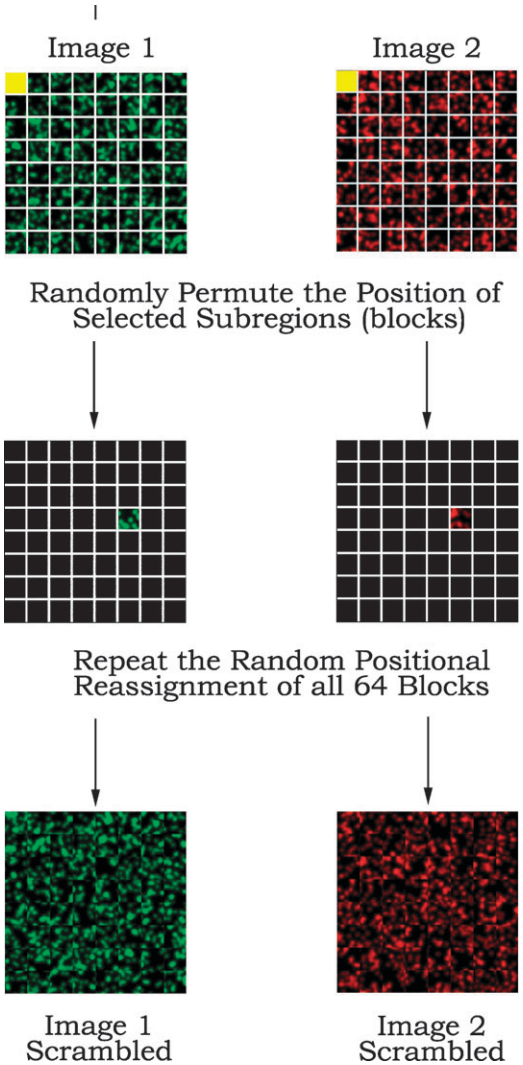

Fig. 4 Image scrambling procedure. Overview of the process leading to the randomization of $Sx \times Sy$ pixel blocks within an $Nx \times Ny$ pixel image. First, the images are evenly divided into $Sx \times Sy$ pixel blocks. In this example there are 64, 32×32 pixel blocks. The first block of both images (highlighted) is randomly assigned a new position within the 8×8 block array. This process is repeated for the remaining blocks within the images until the resulting scrambled images are obtained.

that would normally be included in the overall spatial average used to calculate this point in the correlation function. Therefore, the overall effect on the correlation function of spatially rearranging the image in this manner is to artificially increase the rate at which the function decays to zero, while leaving the zero spatial-lags amplitude unaffected. The degree to which this rate of decay to zero is increased by scrambling depends solely on the size of the pixel scrambling blocks used to create the rearranged image.

Artificially increasing the rate at which the spatial cross-correlation function (and autocorrelation functions) decays to zero aids significantly in resolving its central zero spatial-lags peak from background noise correlation at longer lags. This becomes a considerable advantage when attempting to fit this function in a low spatial sampling situation. For this reason, computer simulation experiments identical to those performed to determine the IF detection limits in ICCS were carried out, except this time, the images were randomly scrambled prior to ICCS analysis in order to see to what extent the effect of scrambling had on lowering the IF detection limit. The results are plotted in Fig. 2 along with the results obtained by simply fitting the spatial correlation functions calculated for the unaltered images as described above.

We can see from Fig. 2 that performing random spatial scrambling of 4×4 pixel blocks within the images prior to ICCS analysis significantly lowered the measured IF detection limits. This observed reduction is entirely due to the increased probability of obtaining a successful fit of the spatial cross-correlation function, calculated after image scrambling. However, there still exists a fundamental detection limit that cannot be overcome by image scrambling. It was found that the measured IF detection limit using the spatial scrambling method was minimized as long as the scrambled block diameter was less than the number of pixels in the e^{-2} radius of the Gaussian convolution function (simulating the laser beam focus radius, ω_0). The 4×4 pixel block size was chosen to provide the maximum advantage in fitting of the reduced-width cross-correlation function, while maintaining a reasonable number of points in the decay of the spatial correlation function to permit fitting.

3.3 Particle distribution

In addition to the NIF sampled within a given image, an equally important parameter that should be considered carefully before applying ICCS to measure interactions is the spatial distribution of the particles themselves. In all of the ICCS measurements presented thus far, it was assumed that the positions of the particles within a given image are randomly distributed from a uniform distribution. The validity of this assumption is most readily assessed through visual inspection of the resulting images. If the spatial distribution of particles in uniform, then the number of particles within each of the small subregions defined by the excitation laser beam area (*i.e.* a single independent spatial fluctuation) will obey Poisson statistics. The amplitude of the 2D spatial auto- and cross-correlation functions calculated for these types of images will be related to the particle density, and the functions will decay to zero over the spatial scale defined by the beam focus (assuming the particles are smaller than the focus size). If, however, the positions of the particles within a given image are not distributed in a random, uniform fashion, then an additional spatial correlation due to this nonuniform particle distribution will result. The spatial autocorrelation function calculated for these images will then consist of contributions from the spatial correlation of this additional, nonuniform particle distribution, and from the underlying spatial correlation of the individual particles that is related to the desired particle densities (see Fig. 6). These additional contributions to the spatial correlation function will, in certain cases, greatly affect its shape, and perturb the subsequent nonlinear least squares fitting. These contributions also influence the relationship between the zero spatial-lags amplitude and the particle number density in a non-trivial way. Not surprisingly, perturbations in either of the two autocorrelation functions due to

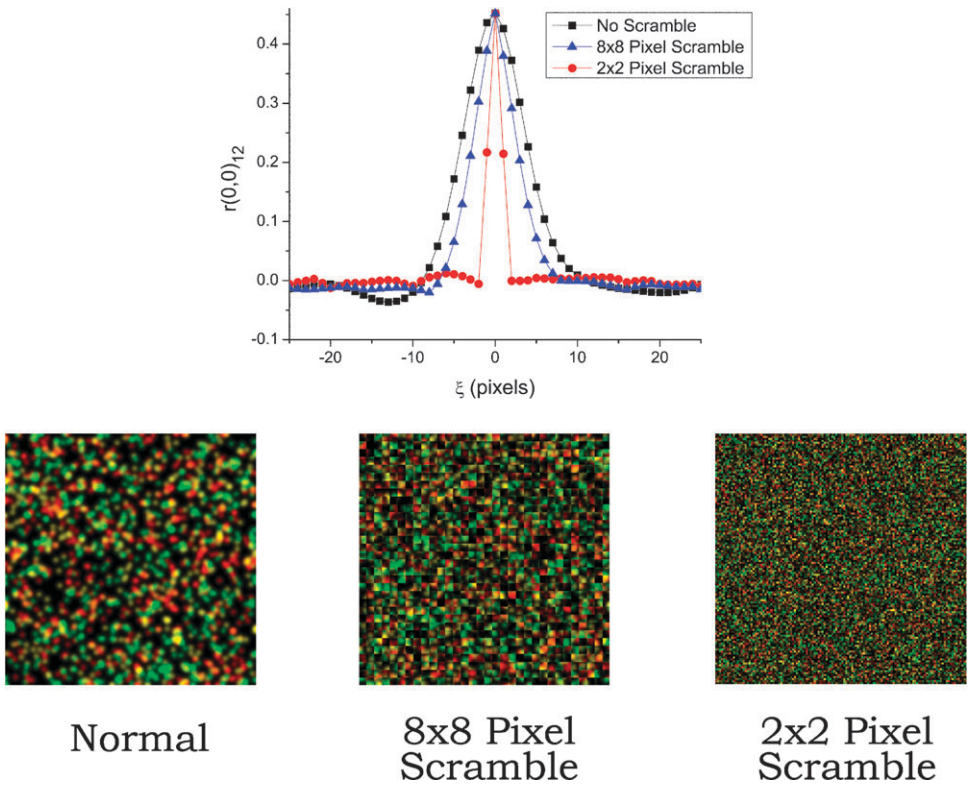

Fig. 5 The effect of random spatial scrambling of individual pixel blocks within a 256 × 256 pixel image on the spatial cross-correlation function calculated for the resulting scrambled images. The IF was set to 0.5 for the simulation. A one-dimensional section of the 2D spatial autocorrelation function through the maximum is shown for clarity. Scrambling does not alter the zero spatial-lags value, $r\ (0, 0)_{11}$, but reduces the value of the function at each successive non-zero spatial lag. Smaller pixel block sizes used for spatial scrambling will increase the rate at which the spatial cross-correlation and autocorrelation functions decay to zero.

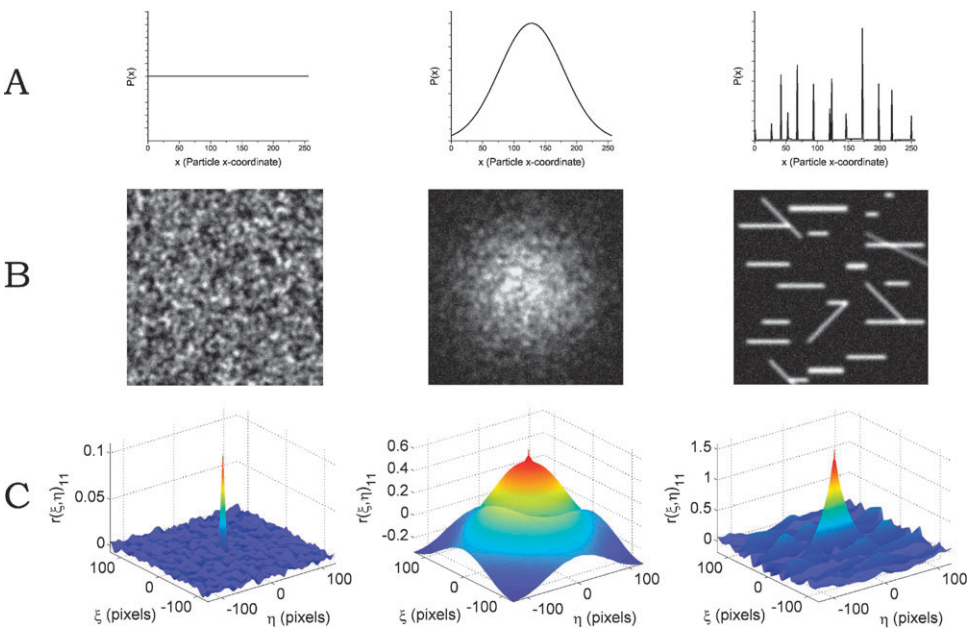

Fig. 6 The effect of uniform and nonuniform spatial distributions of particles on the autocorrelation function. (A) The probability distribution function from which the particle x (and y) coordinates were randomly chosen to create the simulated images shown in (B). The spatial autocorrelation functions calculated for the images are plotted in (C). Background white noise was added to the images, which manifests itself in the autocorrelation functions as a sharp peak augmenting the zero spatial-lags value.

nonuniform particle distributions will also be manifested in the calculated cross-correlation function between the two images.

Nonuniform distributions of fluorescently labelled proteins and other biomolecules in cells are very common, and hence, this presents a difficult challenge for spatial ICS and ICCS analysis of such systems. Typical manifestations of nonuniform particle distributions in cells include large concentration gradients within the imaging region, as well as the formation of large clusters of particles arranged in elongated structures when incorporated into macromolecular complexes (simulated in Fig. 6B).

3.4 ICCS analysis of focal adhesion proteins

Cellular adhesion and migration is largely regulated by a class of heterodimeric transmembrane proteins called integrins. Integrin proteins provide a direct structural link between the extracellular matrix and elements of the cytoskeleton thereby providing 'anchorage' points for attachment and subsequent migration across surfaces. Many different proteins are recruited to these sites of attachment, in addition to integrins, forming large multi-protein complexes, which are collectively referred to as focal adhesions (FAs, see Fig. 1). Integrin proteins act as signaling molecules, by relaying signals that are initiated at the exterior of the cell by the binding of extracellular matrix ligands to the integrins in the membrane, and ultimately passing the signal to the interior of the cell. Integrin receptor proteins have been shown to be involved in the signaling pathways leading to cell growth and differentiation, as well as cell survival and apoptosis.[37]

A complete understanding of the spatial and temporal relationships between the multitude of proteins (*e.g.* talin, α-actinin, paxillin) that comprise FAs is the goal of many current studies. To this end, the study of integrin and integrin-associated proteins is particularly well suited to ICCS analysis because of the fact that the protein is restricted to a planar membrane surface, and because of the relatively slow dynamics of these cell migration proteins that allow for the process to be adequately sampled in time. One major drawback of using spatial ICCS analysis to measure interactions between FA proteins, however, is the spatially nonuniform particle distribution that so often results from the heterogeneous distribution of these complexes in the membrane. As shown in Fig. 6, any deviation from a uniform particle distribution can make the fitting of the autocorrelation and cross-correlation function amplitudes problematic, and hence determination of the interaction fractions, $M1_{\mathrm{ICCS}}$ and $M2_{\mathrm{ICCS}}$, virtually impossible.

Fig. 7A shows an LSM image of YFP–talin fusion protein in a CHO cell plated on a glass coverslip coated with fibronectin, which is the extracellular binding ligand of α_5-integrin proteins. Talin is a protein that is known to bind to the cytosolic tail of the majority of the eight mammalian integrin β subunits, and acts as an intermediary protein that provides a link between the integrin and the cytoskeleton.[38] Recent studies have shown that the binding of talin to the integrin β

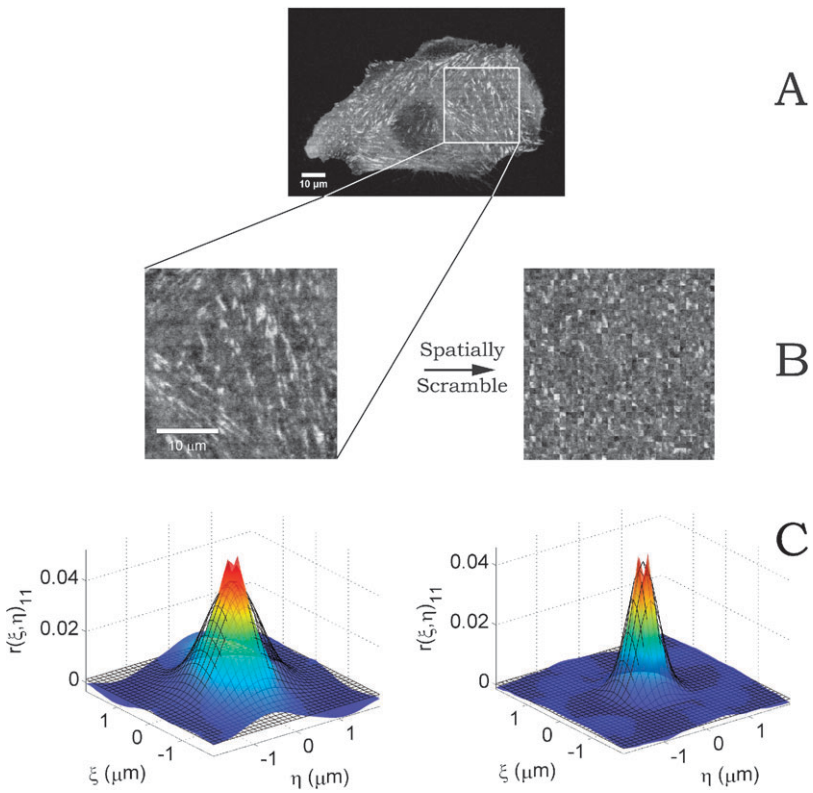

Fig. 7 (A) A confocal LSM image of YFP–talin fusion protein in a CHO–K1 cell. (B) A 256 × 256 pixel region of the cell was selected for spatial correlation analysis. 8 × 8 pixel blocks of the selected subregion were randomly scrambled. The spatial autocorrelation functions calculated for both the image and the scrambled image are shown in (C) along with 2D Gaussian fit functions (mesh). Note the problems with the fit to the correlation function for the unscrambled image due to large focal adhesion structures in the original image.

subunit causes a conformational change in the transmembrane receptor that leads to its activation (*i.e.*, an increase in its affinity for extracellular ligands).[39] It is this integrin activation process that initiates most of the cell signal transduction pathways regulated by integrin proteins.[40]

We can see in Fig. 7A that talin is localized in distinct elongated structures, which are the FAs. It is also clear from the figure that the spatial autocorrelation of the YFP-labelled talin image is not well fit by the 2D Gaussian function and the fit amplitude is underestimated. It was shown that randomly scrambling blocks of pixels within an image can significantly enhance the ability to fit the corresponding cross-correlation function and extract accurate amplitude information in low sampling situations. Similarly, in cases where a nonuniform spatial distribution of particles leads to large perturbations in the Gaussian fitting of the autocorrelation function, spatially scrambling the images prior to correlation analysis will allow for a more reliable estimation of the autocorrelation function amplitude from the fit. This is demonstrated in Fig. 7B where the region of analysis has been divided into 8×8 pixel blocks, the positions of which have been randomly permuted. The corresponding autocorrelation function is shown in solid color and its nonlinear least squares fit (mesh) provides a much better estimate of the correlation function amplitude than the identical analysis on the non-scrambled image. The actual zero spatial-lags point was not weighted in the 2D fit due to the presence of white noise, and is omitted from the plot.

Although the amplitude of the spatial autocorrelation function determined after applying spatial scrambling is a better estimate of the true zero spatial-lags amplitude, it is still difficult to interpret. Due to the fact that the adhesions in this case are $\sim$10 times larger than the excitation laser beam area, conversion of the autocorrelation function amplitude into a more meaningful number density is challenging.[41] In this case, the large spatial intensity fluctuations arising from the presence of the adhesions dominate the cross-correlation function. Image scrambling does in fact aid in extracting the auto- and cross-correlation function amplitudes, but the calculated IFs represent a measure of the cross-correlation between the macroscopic adhesion structures (data not shown). In certain situations the measurement of the IF between large structures as opposed to smaller molecular complexes might be desired. However, if this is not the case, then practical considerations presented in the following section may aid in the measurement of the molecular IF inside the larger multicomponent complexes.

3.5 ICCS analysis of arbitrary regions within images

ICCS analysis is typically performed on small subregions of the acquired two channel images, due in part to nonuniform particle distributions that were discussed in the previous section. In some cases, the actual region of interest may only be a small, or oddly shaped subregion of the cell itself (*e.g.* the leading edge of a migrating cell, Fig. 10). Due to the perturbations of the spatial correlation functions caused by the presence of any 'edges' (spatial fluorescence discontinuities) in the images to be analyzed, it is not always possible to select a completely arbitrary square or rectangular subregion of the image for analysis. These constraints restrict the use of ICCS in a number different situations. Consider the confocal LSM image of a CHO–K1 cell with GFP-labelled α_5-integrin as shown in Fig. 8. Spatial correlation analysis of a rectangular region within the center of the cell will significantly reduce the NIF sampled within the image compared to the case where the entire, circular-shaped cell is selected. Therefore, by selecting the rectangular region on which to apply ICCS, we are effectively throwing away valuable spatial fluctuation information. As we have demonstrated, in many cases it is imperative to perform ICCS analysis on images containing a large NIF, and it is therefore of the utmost importance to retain as many independent spatial fluctuations from the original image as possible.

In ICCS, spatial intensity fluctuations, $\delta i(x,y)_k = i(x,y)_k - \langle i \rangle_k$, recorded at each pixel position are cross-correlated. The fluctuations that are measured for any pixel that has an intensity value equal to the average intensity, $\langle i \rangle_k$, will be zero by definition. Similarly, these pixels will contribute zero to the calculated spatial auto- and cross-correlation functions (eqn (3)). This simple observation can be used to aid in the ICCS analysis of arbitrarily shaped subregions in cells. For instance, if an arbitrary region of the imaged cell is selected, then the resulting matrix can be 'padded' with the mean intensity of the selected pixels to create a final $Nx \times Ny$ image for subsequent ICCS analysis. The number of pixels that are added to the

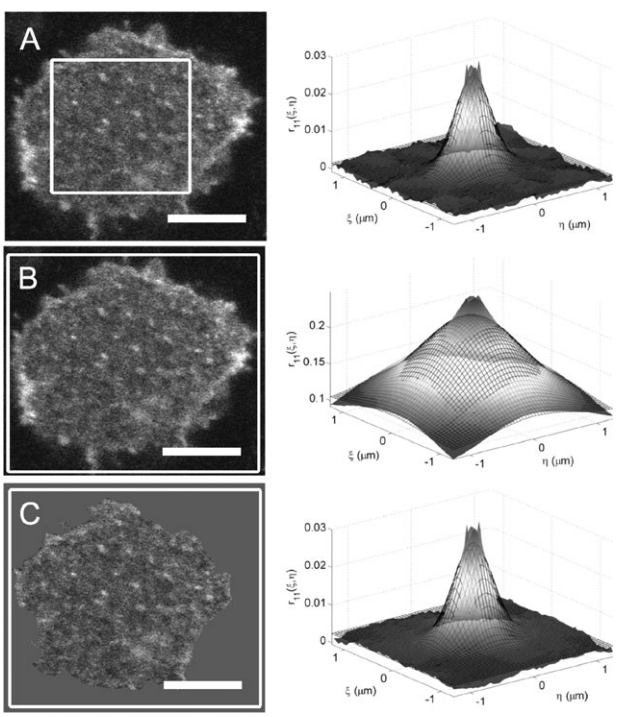

Fig. 8 Confocal LSM images of CHO–K1 cells expressing α_5-integrin–GFP. (A) Spatial autocorrelation analysis of the central region of the cell results in a good fit of the correlation function ($\omega_0 = 0.31$ μm). (B) Spatial autocorrelation analysis of the entire image, including off-cell contributions, results in a poor 2D fit of the correlation function ($\omega_0 = 0.94$ μm). (C) Replacing the background with the mean intensity of the cell leads to a good fit of the autocorrelation function ($\omega_0 = 0.34$ μm). In addition, 62% more NIF were included in (C) than in (A). Scale bar, 5 μm.

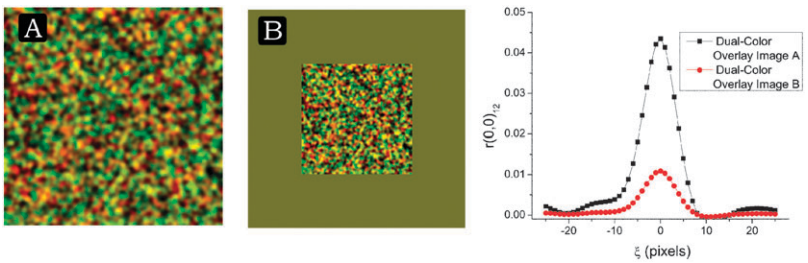

Fig. 9 For each channel of the 256 × 256 pixel two channel overlay image, the respective mean intensities were 'padded' around the outside of the image matrix creating a final 512 × 512 pixel image. The resulting spatial cross-correlation function (and autocorrelation functions) for the 'mean-padded' image is exactly 4 times smaller than that of the original image due to the increased area that was added.

selected region of interest is not important as long as they surround this region to complete a rectangular $Nx \times Ny$ pixel array. From the equation for the spatial auto- and cross-correlation functions given above and in eqn (3), one can see that any 'padding' of the selected region of interest with its average intensity will not contribute to the numerator of the spatial correlation functions, but will in fact, decrease the entire function by a factor that is proportional to the number of pixels that were added to the image (Fig. 9).

This decrease occurs because we have artificially introduced additional spatial lag values to be included in the spatial averaging that is performed when calculating the correlation functions. This is easily accounted for, however, and in cross-correlation experiments, where we are only interested in the ratio of the cross-correlation function amplitude to that of the autocorrelation function, no adjustments are necessary because this ratio will remain unchanged. Arbitrary subregions of images can now be analyzed by simply 'padding' the resulting selection with the mean intensity of the fluorescence signal of the selected subregion. Normal ICCS analysis of such images will then result in accurate IF measurements.

This method for selecting arbitrary subregions within images was applied to two channel total internal reflection fluorescence (TIRF) microscopy images in order to measure the IF between the cytoskeletal protein, actin, and one of its binding partners α-actinin. The α-actinin protein constitutes an important component of FAs by linking intracellular actin filaments to transmembrane integrin receptors, thus coupling the cytoskeleton to the extracellular matrix.[42,43] While these two proteins are known to interact, less is known about the fraction of interacting molecules, especially in different regions of the cell.

In order to measure the interaction between actin and α-actinin at the leading edge of a migrating cell (outside of well-formed FAs), a small subregion of the two channel TIRF image (α-actinin–GFP and actin–mRFP) was manually selected at the cell front. The mean intensity of this small subregion was then used to 'pad' the surrounding regions to create two images with a total size of 256 pixels (Fig. 10). 4 × 4 pixel sub-blocks of these images were then randomly spatially scrambled and ICCS analysis was performed on the resulting images. It was found that there was significant interaction between actin–mRFP and α-actinin–GFP in this manually selected region ($M1_{ICCS}$ = 0.71 and $M2_{ICCS}$ = 0.62). This demonstrates that the extension of ICCS analysis to manually selected image subregions is possible in two channel fluorescence images, which can be an important tool in measuring molecular interactions in subregions within cells with heterogeneous distributions of proteins.

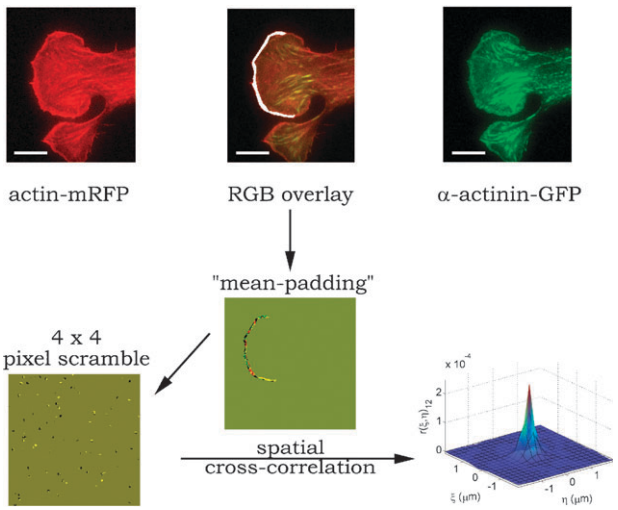

Fig. 10 The interaction of actin and α-actinin at the leading edge of a migrating cell. The interaction of actin and α-actinin at the leading edge of a migrating cell. A cellular subregion within the two channel TIRF microscopy overlay image of actin–mRFP and α-actinin–GFP was manually selected (white area). Pre-processing of the images by mean-padding, and spatial sub-block scrambling was carried out prior to ICCS analysis to determine the IFs between the two proteins *via* ICCS ($M1_{ICCS}$ = 0.71 and $M2_{ICCS}$ = 0.62). Scale bars are 10 μm. Images courtesy of Prof. Rick Horwitz.

Selection of arbitrary regions of interest within the image in this manner significantly increases the range of images to which ICCS can be applied. Combined with random scrambling of pixel blocks within the image, the 'mean-padding' procedure allows for small numbers of interacting particles in small user-defined regions of the cell to be measured with relative ease using ICCS, which would be extremely difficult to measure without the use of such tools. These simple methods for overcoming some of the inherent limitations in the ICCS technique have extended its practical application to measuring interactions in cells.

5. Conclusions

Spatial ICCS is a powerful tool for measuring interactions between macromolecules in cells *via* fluorescence microscopy

image analysis, especially when the particle number density is high. In fact, ICCS is sensitive to any type of spatial molecular association, whether it is mediated through a covalent or electrostatic interaction, or *via* an unlabelled intermediary protein as part of a larger complex. However, certain limitations such as the relatively high IF detection limit and the need for uniform particle distributions, have remained a significant obstacle for the application of spatial ICCS analysis to many biological systems. In this work, we have developed two strategies to extend the scope of spatial ICCS analysis, and to significantly improve the practical usage of the technique. First, the random scrambling of small sub-blocks within the image and second, the mean-padding procedure for arbitrary sub-region selection.

The IF detection limits of ICCS can limit the effectiveness of the method in many experimental situations and these are strongly dependent on the NIF sampled within the image. However, it was shown that dividing the image into smaller $Sx \times Sy$ pixel sub-blocks and randomly redistributing these blocks throughout the entire $Nx \times Ny$ image, dramatically improved the fit quality for the calculated spatial cross-correlation function for images with low NIF sampling, thereby, decreasing the IF detection limits. The random scrambling of smaller sub-blocks within the image increases the rate at which the spatial cross-correlation (and autocorrelation) function decays to zero, but does not affect the zero spatial-lags amplitude. The net result is a narrowing of the correlation functions, which increases the chance of obtaining a good fit to the 2D Gaussian function because it leads to better spatial resolution of the central peak from random background correlations. The use of this scrambling method was also shown to extend the application of ICCS to the measurement of the colocalization within large, irregularly shaped objects within the images, such as focal adhesions that normally would preclude the application of ICCS.

We introduced a procedure to select arbitrary regions of the images for analysis. This procedure consisted of 'padding' the matrix that contained the selected region of interest with the mean intensity of that region. ICCS analysis of these types of images resulted in identical spatial correlation functions, reduced by a factor proportional to the number of pixels that were added around the region of interest. This practical tool, combined with the image scrambling procedure, allows one to select individual focal adhesions, cell protrusions, or other small regions of interest for subsequent ICCS analysis of the molecular interactions within these structures. Selection of arbitrary regions of interest within the image in this manner significantly increases the range of systems to which ICCS can be applied. Combined with random scrambling of pixel blocks within the image, the mean-padding procedure allows for low numbers of interacting particles in small user-defined regions of the cell to be measured with relative ease using ICCS. This would be extremely difficult to measure without the use of such tools. We have shown that simple methods for overcoming some of the inherent limitations in the ICCS technique have extended its practical application for measuring protein interactions in cells. Due to the statistical nature of spatial ICCS, certain limitations persist such as the requirement of relatively large areas of analysis. This implies that spatial ICCS cannot be applied to arbitrarily small subregions within a cell as would be necessary in the case of images of neuronal dendrites or bacteria. In addition, the application of ICCS results in a measure of the degree to which two molecules are spatially associated and is therefore only an indirect measure of interaction. As such, other *in situ* techniques such as FRET together with *in vitro* co-immunoprecipitation studies are necessary to confirm the direct interaction of the two molecules of interest.

Finally, we have presented a method to quantify the interaction of cellular components from fluorescence images collected at a given time. However, to gain more insight into the important temporal relationships between these components, temporal ICCS and related techniques must be performed on two-channel time series to measure the co-transport of these proteins.

6. Experimental

6.1 Simulated images

All the image simulations and correlation function calculations were performed using custom written MATLAB 7.0 (The MathWorks, Natick, MA) routines and the image processing and optimization toolboxes. These routines are freely available at http://wisemangroup.mcgill.ca/software.php. Details of the simulations and analysis have been published previously.[21]

6.2 Transfection of fluorescent protein constructs

CHO–K1 cells (Sigma-Aldrich, St. Louis, MO) were cultured in Dulbecco's modified Eagle's medium supplemented with 10% fetal bovine serum, 4 mM L-glutamine, 100 units mL^{-1} penicillin, 0.1 mg mL^{-1} streptomycin, and 0.1 mM nonessential amino acids (Gibco, Carlsbad, CA). Cells were maintained in a humidified 5.0% CO_2 atmosphere at 37 °C. Cells were plated on 6-well dishes (VWR, Mississauga, ON) and grown for 2 days. Two solutions were prepared for each well to be transfected (12 solutions total). The first set of solutions was prepared by diluting 5 μL of lipofectamine (Invitrogen, Carlsbad, CA) in 50 μL of OptiMEM (Invitrogen). The second set of solutions was prepared by diluting 1 μL DNA plasmid encoding for YFP–talin (Prof. Horwitz Lab, University of Virginia) in 50 μL OptimMEM. These two sets of solutions were mixed and left at room temperature for 20 min. The resulting 100 μL lipofectamine–DNA solutions were then added to the 6-well plates containing the cells, and were incubated for 6 h at 37 °C, and 5.0% CO_2. After the 6 h incubation time, the liquid was removed from each well and replaced with normal growth media. After 25 h, the cells were removed from the surface of the 6-well plate by addition of a 0.25% (w/v) trypsin solution. The cells were then incubated at 37 °C on 35 mm microwell dishes (MatTek, Ashland MA) that had been coated with fibronectin. These dishes were coated by incubation for 1 h at 37 °C with a 2 μg mL^{-1} solution of fibronectin in PBS. The cells were then fixed with a 4% (w/v) paraformaldehyde solution for 10 min at room temperature and then imaged. MEF cells were cultured and transfected as

described previously.[44] Stable α_5–GFP transfected cell lines were generously provided by Prof. R. Horwitz.

6.3 Microscopy

The CHO cells expressing YFP–talin were imaged using a FV300 Olympus (Olympus America, Melville, NY) confocal LSM. Excitation of YFP was provided by the 514 nm laser line of an Ar ion laser. The resulting fluorescence emission was collected with an Olympus 60× PlanApo oil immersion objective (NA 1.4). Wavelengths between 535 nm and 565 nm were selected using a band-pass emission filter (Chroma, Rockingham, VT) and detected using a photomultiplier tube with a voltage of 550 V. The pixel resolution of these images was 0.12 μm. The TIRF system used to image actin–mRFP and α-actinin–EGFP was described in detail previously.[44] Confocal imaging of α_5–GFP CHO–K1 cells was described previously.[20]

Acknowledgements

Many thanks to Jessica Zareno and Colin Choi under the supervision of Prof. Rick Horwitz at the University of Virginia for providing the YFP–talin plasmid and for performing the TIRF imaging of α-actinin–GFP/actin–mRFP. DLK acknowledges an NSERC CGS fellowship, and PWW acknowledges grants from NSERC, CIHR, and CFI. This work was also supported by funding from NIGMS grants GM23244 and U54 GM64346 and the Cell Migration Consortium.

References

1 K. H. Young, Yeast two-hybrid: So many interactions, (in) so little time. . ., *Biology of Reproduction*, 1998, **58**, 302–311.
2 S. Fields and O.-K. Song, A novel genetic system to detect protein–protein interactions, *Nature*, 1989, **340**(6230), 245–246.
3 R. Zaidel-Bar, S. Itzkovitz, A. Ma'ayan, R. Iyengar and B. Geiger, Functional atlas of the integrin adhesome, *Nat. Cell Biol.*, 2007, **9**(8), 858–867.
4 P. Uetz, L. Giot, G. Cagney, T. A. Mansfield, R. S. Judson, J. R. Knight, D. Lockshon, V. Narayan, M. Srinivasan, P. Pochart, A. Qureshi-Emili, Y. Li, B. Godwin, D. Conover, T. Kalbfleisch, G. Vijayadamodar, M. Yang, M. Johnston, S. Fields and J. M. Rothberg, A comprehensive analysis of protein–protein interactions in *Saccharomyces cerevisiae*, *Nature*, 2000, **403**(6670), 623–627.
5 T. Ito, T. Chiba, R. Ozawa, M. Yoshida, M. Hattori and Y. Sakaki, A comprehensive two-hybrid analysis to explore the yeast protein interactome, *Proc. Natl. Acad. Sci. U. S. A.*, 2001, **98**, 4569–4574.
6 C. M. Deane, L. Salwiński, I. Xenarios and D. Eisenberg, Protein interactions: two methods for assessment of the reliability of high throughput observations, *Mol. Cell. Proteomics*, 2002, **1**(5), 349–356.
7 E. Sprinzak, S. Sattath and H. Margalit, How reliable are experimental protein–protein interaction data?, *J. Mol. Biol.*, 2003, **327**, 919–923.
8 I. Stagljar and S. Fields, Analysis of membrane protein interactions using yeast-based technologies, *Trends Biochem. Sci.*, 2002, **27**, 559–563.
9 D. A. Calderwood, Integrin activation, *J. Cell Sci.*, 2004, **117**(5), 657–666.
10 R. De Francesco, A. Pastore, G. Vecchio and R. Cortese, Circular dichroism study on the conformational stability of the dimerisation domain of the transcriptional factor LFB1, *Biochemistry*, 1991, **30**(1), 143–147.
11 D. Grunwald, M. C. Cardoso, H. Leonhardt and V. Buschmann, Diffusion and binding properties investigated by fluorescence correlation spectroscopy (FCS), *Curr. Pharm. Biotechnol.ogy*, 2005, **6**(5), 381–386.
12 P. Schuck, Reliable determination of binding affinity and kinetics using surface plasmon resonance biosensors, *Curr. Opin. Biotechnol.*, 1997, **8**(4), 498–502.
13 M. Doyle, Characterization of binding interactions by isothermal titration microcalorimetry, *Curr. Opin. Biotechnol.*, 1997, **8**(1), 31–35.
14 R. W. Kriwacki, J. Wu, G. Siuzdak and P. E. Wright, Probing protein/protein interactions with mass-spectrometry and isotropic labelling-analysis of the p21/cdk2 complex, *J. Am. Chem. Soc.*, 1996, **118**(22), 5320–5321.
15 S. Sánchez-Carrascoa, J. G. Delcros, A. A. Moya-García, F. Sánchez-Jiménez and Ramírez, Study by optical spectroscopy and molecular dynamics of the interaction of acridinespermine conjugate with DNA, *Biophys. Chem.*, 2008, **133**, 54–65.
16 G. J. Thomas, Jr, Raman spectroscopy of protein and nucleic acid assemblies, *Annu. Rev. Biophys. Biomol. Struct.*, 1999, **28**, 1–27.
17 R. P. Gonçalves, G. Angus, P. Sens, C. Houssin, B. Bartenlian and S. Scheuring, Two-chamber AFM: probing membrane proteins separating two aqueous compartments, *Nat. Methods*, 2006, **3**(12), 1007–1012.
18 K. Truong and M. Ikura, The use of FRET imaging microscopy to detect protein–protein interactions and protein conformational changes *in vivo*, *Curr. Opin. Struct. Biol.*, 2001, **11**, 573–578.
19 E. M. M. Manders, F. J. Verbeek and J. A. Aten, Measurement of co-localization of objects in dual color confocal images, *J. Microsc.*, 1993, **169**, 375–382.
20 S. Costantino, J. W. D. Comeau, D. L. Kolin and P. W. Wiseman, Accuracy and dynamic range of spatial image correlation and cross-correlation spectroscopy, *Biophys. J.*, 2005, **89**, 1251–1260.
21 J. W. D. Comeau, S. Costantino and P. W. Wiseman, A Guide to Accurate Colocalization Measurements, *Biophys. J.*, 2006, **91**, 4611–4622.
22 S. V. Costes, D. Daelemans, E. H. Cho, Z. Dobbin, G. Pavlakis and S. Lockett, Automatic and quantitative measurement of protein–protein colocalization in live cells, *Biophys. J.*, 2004, **86**(6), 3993–4003.
23 D. Magde, E. Elson and W. W. Webb, Thermodynamic fluctuations in a reacting system—measurement by fluorescence correlation spectroscopy, *Phys. Rev. Lett.*, 1972, **29**(11), 705–708.
24 E. L. Elson and D. Magde, Fluorescence correlation spectroscopy. I. Conceptual basis and theory, *Biopolymers*, 1974, **13**, 1–27.
25 D. Magde, E. L. Elson and W. W. Webb, Fluorescence correlation spectroscopy. II. An experimental realization, *Biopolymers*, Jan 1974, **13**(1), 29–61.
26 J. L. Swift, M. C. Burger, D. Massotte, T. E. Dahms and D. T. Cramb, Two-photon excitation fluorescence cross-correlation assay for ligand–receptor binding: cell membrane nanopatches containing the human micro-opioid receptor, *Anal. Chem.*, 2007, **79**, 6783–6791.
27 K. G. Heinze, A. Koltermann and P. Schwille, Simultaneous two-photon excitation of distinct labels for dual-color fluorescence cross-correlation analysis, *Proc. Natl. Acad. Sci. U. S. A.*, 2000, **97**, 10377–10382.
28 J. Widengren and R. Rigler, Fluorescence correlation spectroscopy as a tool to investigate chemical reactions in solutions and on cell surfaces, *Cell. Mol. Biol.*, 1998, **44**, 857–879.
29 Petra Schwille, U. Haupts, S. Maiti and W. W. Watt, Molecular dynamics in living cells observed by fluorescence correlation spectroscopy with one- and two-photon excitation, *Biophys. J.*, 1999, **77**, 2251–2265.
30 N. O. Petersen, P. L. Hoddelius, P. W. Wiseman, O. Seger and K. E. Magnusson, Quantitation of membrane receptor distributions by image correlation spectroscopy: concept and application, *Biophys. J.*, Sep 1993, **65**(3), 1135–46.
31 P. W. Wiseman and N. O. Petersen, Image correlation spectroscopy. II. Optimization for ultrasensitive detection of pre-existing platelet-derived growth factor-beta receptor oligomers on intact cells, *Biophys. J.*, Feb. 1999, **76**(2), 963–77.
32 S. A. Kim, K. G. Heinze, K. Bacia, M. N. Waxham and P. Schwille, Two-photon cross-correlation analysis of intracellular reactions with variable stoichiometry, *Biophys. J.*, 2005, **88**(6), 4319–4336.

33 P. W. Wiseman, J. A. Squier, M. H. Ellisman and K. R. Wilson, Two-photon image correlation spectroscopy and image cross-correlation spectroscopy, *J. Microsc.*, 2000, **200**(1), 14–25.
34 D. L. Kolin and P. W. Wiseman, Advances in Image Correlation Spectroscopy: Measuring Number Densities, Aggregation States, and Dynamics of Fluorescently labeled Macromolecules in Cells, *Cell Biochem. Biophys.*, 2007, **49**(3), 141–164.
35 P. Schwille, Cross-correlation analysis in FCS, in *Fluorescence Correlation Spectroscopy: Theory and Applications*, ed. R. Rigler and E. S. Elson, Springer, 2001, pp. 360–378.
36 E. M. M. Manders, Chromatic shift in multicolour confocal microscopy, *J. Microsc.*, 1996, **185**, 321–328.
37 R. Hynes, Integrins: Bidirectional, allosteric signaling machines, *Cell*, 2002, **110**(6), 673–687.
38 D. R. Critchley, Focal adhesions—the cytoskeletal connection, *Curr. Opin. Cell Biol.*, 2000, **12**(1), 133–139.
39 S. Tadokoro, S. J. Shattil, K. Eto, V. Tai, R. C. Liddington, J. M. de Pereda, M. H. Ginsberg and D. A. Calderwood, Talin binding to integrin β tails: a final common step in integrin activation, *Science*, 2003, **302**(5642), 103–106.
40 B. I. Ratnikov, A. W. Partridge and M. H. Ginsberg, Integrin activation by talin, *J. Thromb. Haemost.*, 2005, **3**(8), 1783–1790.
41 K. Starchev, J. Zhang and J. Buffle, Applications of fluorescence correlation spectroscopy-particle size effect, *J. Coll. Inter. Sci.*, 1998, **203**(1), 189–196.
42 M. Vicente-Manzanares, D. J. Webb and A. R. Horwitz, Cell migration at a glance, *J. Cell Sci.*, 2005, **118**, 4917–4919.
43 C. M. Laukaitis, D. J. Webb, K. Donais and A. F. Horwitz, Differential dynamics of α5-integrin, paxillin, and α-actinin during formation and disassembly of adhesions in migrating cells, *J. Cell Biol.*, 2001, **153**(7), 1427–1440.
44 C. M. Brown, B. Hebert, D. L. Kolin, J. Zareno, L. Whitmore, A. R. Horwitz and P. W. Wiseman, Probing the integrin-actin linkage using high resolution protein velocity mapping, *J. Cell Sci.*, 2006, **119**, 5204–5214.